ISSN 1063-7761, Journal of Experimental and Theoretical Physics, 2017, Vol. 124, No. 5, pp. 792–804. © Pleiades Publishing, Inc., 2017.
Original Russian Text © E.V. Eremin, N.V. Volkov, K.A. Sablina, O.A. Bayukov, M.S. Molokeev, V.Yu. Komarov, 2017, published in Zhurnal Eksperimental'noi i Teoreticheskoi Fiziki, 2017, Vol. 151, No. 5, pp. 930–943.

ORDER, DISORDER, AND PHASE TRANSITION IN CONDENSED SYSTEM

Analysis of the Exchange Magnetic Structure in $Pb_3Mn_7O_{15}$

E. V. Eremin[a,b]*, N. V. Volkov[a,b], K. A. Sablina[a], O. A. Bayukov[a], M. S. Molokeev[a], and V. Yu. Komarov[c,d]

[a] *Kirensky Institute of Physics, Siberian Branch, Russian Academy of Sciences, Krasnoyarsk, 660036 Russia*
[b] *Siberian Federal University, Krasnoyarsk, 660041 Russia*
[c] *Nikolaev Institute of Inorganic Chemistry, Siberian Branch, Russian Academy of Sciences, pr. Akademika Lavrent'eva 3, Novosibirsk, 630090 Russia*
[d] *Novosibirsk State University, ul. Pirogova 2, Novosibirsk, 630090 Russia*
**e-mail: eev@iph.krasn.ru*

Received November 9, 2016

Abstract—The indirect-coupling model is used to analyze the exchange magnetic structure of $Pb_3Mn_7O_{15}$ in the hexagonal setting. The ratios of manganese ions Mn^{4+}/Mn^{3+} in each nonequivalent position are determined. $Pb_3(Mn_{0.95}Ge_{0.05})_7O_{15}$ and $Pb_3(Mn_{0.95}Ga_{0.05})_7O_{15}$ single crystals are grown by the solution–melt method in order to test the validity of the proposed model. The structural and magnetic properties of the single crystals are studied. The magnetic properties of the grown single crystals are compared with those of nominally pure $Pb_3Mn_7O_{15}$.

DOI: 10.1134/S1063776117040112

1. INTRODUCTION

Among the oxide compounds, manganites with the variable valence of manganese ions have been interesting and challenging objects over several decades. A rich set of their physical properties caused by charge, spin, and orbital degrees of freedom and the possibility of controlling these properties make these materials promising for both a fundamental investigation and a wide practical application [1].

Manganites with a perovskite structure $R_{1-x}A_xMnO_3$ (R = rare-earth metal, A = Ca, Sr, Ba, Pb) are mainly studied in a systematic manner. The diverse unusual physical phenomena detected in impurity-containing perovskite manganites, the mechanisms of which are still poorly understood, stimulate an active search and investigation of other oxide families, which contain manganese ions in a mixed valence state and have no perovskite structure.

The compound $Pb_3Mn_7O_{15}$, which contains manganese ions having various oxidation levels, has been extensively studied in recent years. Its thermodynamic [2, 3], dielectric [4], and structural [5, 6] properties have recently been investigated. Specific feature were detected in the temperature dependence of magnetization at $T_1 = 160$ K, $T_2 = 70$ K, and $T_3 = 25$ K [2], and they agree well with the anomalies in the temperature dependence of heat capacity [3]. A cluster-type order with a characteristic broad peak in the temperature dependence of magnetization is considered to take place at temperature T_1, a long-range magnetic order appears in the system at T_2, and a spin-reorientation transition occurs at T_3. When the temperature decreases in the range 150–210 K, charge ordering takes place, which is indicated by the anomalies in the temperature dependences of complex permittivity [4].

The structural studies [5] performed on a synchrotron in the temperature range 15–295 K showed that $Pb_3Mn_7O_{15}$ has an orthorhombic structure with space group *Pnma*. It was found later [6] that, upon heating, the orthorhombic structure of space group *Pnma*, which exists at room temperature, transforms first into a spatially modulated structure (at $T_{s1} = 400$ K) and, then (at $T_{s2} = 560$ K), into a hexagonal structure with space group $P6_3/mcm$. As was shown in [7], the hexagonal–orthorhombic transition occurs due to orbital and charge ordering when temperature decreases.

Despite numerous works dealing with this compound, its magnetic structure is still poorly understood. Unfortunately, this magnetic structure has not been studied by neutron diffraction. However, even such studies will be performed, identification will require much efforts. The unit cell of the orthorhombic *Pnma* phase has eight formula units and manganese ions are located at nine nonequivalent sites. Moreover, the magnetic structure undergoes geometric frustrations and, hence, should be complex.

The growth of $Pb_3Mn_7O_{15}$ crystals with the addition of various magnetic ions leads to a substantial change in their transport, magnetic, and structural

properties. For example, the magnetic properties change substantially when iron ions substitute for manganese ions in $Pb_3(Mn_{1-x}Fe_x)_7O_{15}$ at a doping level $x > 0.1$ [8]. The broad peak at $T_1 = 160$ K disappears, a long-range magnetic order does not appear, and the temperature dependences of magnetization at low temperatures demonstrate signs of spin glass with a characteristic divergence of magnetization under various cooling conditions (with and without a magnetic field). In contrast to $Pb_3Mn_7O_{15}$ samples (where hysteretic magnetization curves are only observed for an in-plane magnetic field), the field dependences of samples with $x > 0.1$ have the same shape irrespective of the direction of an applied magnetic field; that is, the magnetic characteristics of these samples have an isotropic character. The solidified phase has a hexagonal system and space group $P6_3/mcm$ [8].

Similar behavior was observed when $4d$ Rh^{3+} ions substitute for manganese ions [9]. The corresponding crystal structure also has space group $P6_3/mcm$ and the magnetic order in $Pb_3(Mn_{1-x}Rh_x)_7O_{15}$ disappears at a doping level $x > 0.5$.

Another situation is observed when nickel ions substitute for manganese ions. The crystal structure also changes in $Pb_3Mn_{5.5}Ni_{1.5}O_{15}$. This compound has space group $P3c1$. The magnetic ordering temperature changes weakly ($T_2 = 65$ K) but the broad peak in the temperature dependence of magnetization at $T_1 = 160$ K disappears [10].

Obviously, doping of $Pb_3Mn_7O_{15}$ by magnetic ions leads to the following two effects. First, the integrals of exchange interactions between magnetic ions change because of spatial deformations; second, the ratio of manganese ions Mn^{3+}/Mn^{4+} can change, which should result in more substantial complication of the magnetic structure.

Thus, the purpose of this work is to study the sequential substitution of nonmagnetic ions Ga^{3+} and Ge^{4+} for manganese ions to clarify the exchange magnetic structure of $Pb_3Mn_7O_{15}$. This type of substitution makes it possible to partly exclude first Mn^{3+} ions and then Mn^{4+} ions from consideration.

2. EXPERIMENTAL

Manganite $Pb_3(Mn_{0.95}Ga_{0.05})_7O_{15}$ and $Pb_3(Mn_{0.95}Ge_{0.05})_7O_{15}$ single crystals were grown by solidification from a molten solution. As the solution, we used PbO, which is known as an effective solvent for many oxide compounds and makes it possible to avoid the incorporation of uncontrollable impurities into the lattice matrix. The synthesis of the single crystals started from heating of a mixture of oxides PbO, Mn_2O_3, and Ga_2O_3 (GeO_2) in a platinum crucible to a temperature $T \approx 1000$°C in 4 h. The crucible was then slowly cooled to 900°C at a rate of 2 K/h. The furnace was then turned off and cooled to room temperature. The grown single crystals were mechanically removed and had the shape of black hexagonal plates 20 mm in diameter and about 1 mm in thickness.

X-ray diffraction (XRD) experiments were carried out on a single-crystal Bruker x8 APEXII diffractometer using monochromatized MoK_α radiation (λ = 0.7106 Å) at room temperature.

The magnetic properties of the grown single crystals were measured on a PPMS-9 (QuantumDesign) vibrating-sample magnetometer in the temperature range 4.2–300 K and magnetic fields up to 9 T.

3. EXPERIMENTAL RESULTS

3.1. Structural Properties

XRD experiments were performed on $Pb_3Mn_7O_{15}$, $Pb_3Mn_7O_{15}$:Ga^{3+}, and $Pb_3Mn_7O_{15}$:Ge^{4+}. The orientation matrix and the unit cell parameters were determined using all strong ($I > 2\sigma(I)$) lines. The unit cells corresponded to the orthorhombic system of space group *Pnma*, as was detected earlier [6]. The main crystallographic characteristics and the experimental parameters are given in Table 1, and the atomic coordinates are presented in Table 2.

An experimental model was directly searched for using the SHELXS software package by a direct method [11]. As a result, the coordinates of all atoms were found. The obtained structural model was refined by the least squares method using the SHELXL97 software package.

Since the proposed concentration of Ge^{4+} ions in $Pb_3Mn_7O_{15}$:Ge^{4+} or Ga^{3+} in $Pb_3Mn_7O_{15}$:Ga^{3+} is low, it would be very unstable to refine the position occupancy for nine independent Mn atoms. Therefore, the presence of Ge^{4+} and Ga^{3+} was not taken into account in the model. Since the ionic radii IR(Ge^{4+}, CN = 6) = 0.53 Å and IR(Mn^{4+}, CN = 6) = 0.53 Å are identical and the ionic radii IR(Ga^{3+}, CN = 6) = 0.62 Å and IR(Mn^{3+}, CN = 6) = 0.58–0.645 Å are very close to each other [12], an analysis of the d(Mn–0) bond lengths also cannot help us to find the positions of ions Ge^{4+} and Ga^{3+} in the structure. Nevertheless, we can assume that Ge^{4+} is most likely to substitute for Mn^{4+} rather than Mn^{3+}, since the excess positive charge has to be compensated by vacancies in the latter case for the total charge of the cell to be zero. A similar situation takes place with Ga^{3+}, which should predominantly occupy the positions of Mn^{3+} rather than Mn^{4+}.

To find the positions to be occupied by the Mn^{3+} and Mn^{4+} ions in the $Pb_3Mn_7O_{15}$:Ge^{4+} and $Pb_3Mn_7O_{15}$:Ga^{3+} compounds, we calculated the average d(Mn–O) bond lengths for each position (Figs. 1a, 1b) and the sum of the valence forces (Figs. 1c, 1d) using the tabulated data from [13]. According to these data, we can state that the structure has a least twp positions (Mn2, Mn3) predominantly

Table 1. Basic crystallographic characteristics and experimental parameters

	Crystallographic data		
Compound	$Pb_3Mn_7O_{15}$	$Pb_3Mn_7O_{15}$:Ge^{4+}	$Pb_3Mn_7O_{15}$:Ga^{4+}
Space group, Z	*Pnma*, 8	*Pnma*, 8	*Pnma*, 8
a, Å	13.610 (1)	13.6115 (9)	13.6006 (3)
b, Å	17.325 (1)	17.350 (1)	17.3368 (4)
c, Å	10.0290 (8)	10.0172 (6)	10.0118 (3)
V, Å^3	2364.7 (3)	2365.7 (3)	2360.7 (1)
D_x, mg/m^3	7.001	6.998	7.012
μ, mm^{-1}	49.842	49.821	49.927
	Data acquisition parameters		
Data acquisition parameters	8552	43215	25171
Number of independent reflections, N_1	4417	4860	3856
Number of reflections with $I > 2\sigma(I)$, N_2	3340	3653	2895
With allowance for absorption	Multiscanning		
R_{int}	0.0276	0.0386	0.0773
$2\theta_{max}$	65.16°	69.09°	62.07°
H, K, L	$-20 \to 20$, $-26 \to 26$, $-15 \to 15$	$-20 \to 17$, $-27 \to 22$, $-15 \to 14$	$-16 \to 19$, $-24 \to 25$, $-14 \to 14$
	Refined results		
R [for N_2 reflections]	0.0839	0.0891	0.0736
R [for N_1 reflections]	0.1042	0.1088	0.0921

occupied by Mn^{3+} ions and three positions (Mn1, Mn6, Mn7) predominantly occupied by Mn^{4+} ions. The other four positions (Mn4, Mn5, Mn8, Mn9) are most likely to be occupied by both ions. Since Ge^{4+} ions were assumed to substitute for Mn^{4+} ions, they should be mainly located in layers (Fig. 1e). In contrast Ga^{3+} ions should be predominantly located in columns between the layers (Fig. 1f).

3.2. Magnetic Properties

As follows from the XRD data, the addition of Ga^{3+} and Ge^{4+} ions to $Pb_3Mn_7O_{15}$ weakly changes the initial structure. Therefore, all manganese ions Mn^{3+} and Mn^{4+} are assumed to be retained at the same positions as before substitution except for the ions displaced by gallium and germanium ions.

Figure 2 shows the temperature dependences of the magnetizations of the $Pb_3(Mn_{0.95}Ge_{0.05})_7O_{15}$ and $Pb_3(Mn_{0.95}Ga_{0.05})_7O_{15}$ single crystals in comparison with $Pb_3Mn_7O_{15}$. The measurements were performed upon cooling in a magnetic field $B = 0.05$ T directed along axis a (normal to the layers of oxygen octahedra (Fig. 1)) and in plane bc.

The temperature dependence of the magnetization of $Pb_3Mn_7O_{15}$ has a small strongly broadened peak at $T_1 = 160$ K when temperature decreases (Fig. 2a, inset). The nature of this anomaly is still poorly understood, and it is likely to be related to the appearance of cluster ordering. When temperature decreases further, a long-range magnetic order with a weak spontaneous magnetic moment lying in the crystal plane appears in the system at $T_2 = 72$ K (the maximum magnetic moment is seen to be $0.14\mu_B$/formula unit at $T = 4.2$ K; see Fig. 2a). A spin-reorientation transition is likely to occur at $T_3 = 25$ K; however, its nature is beyond the scope of this investigation. The paramagnetic Curie temperature determined from the inverse dependence of susceptibility is $\theta = -590$ K, and the effective magnetic moment is $13.3\mu_B$/formula unit [2]. The theoretically calculated moment ($11.9\mu_B$/formula unit provided $g_J = 2$) is slightly lower than the experimental value. Table 3 gives the parameters determined from the temperature dependence of the magnetic susceptibility for $Pb_3Mn_7O_{15}$, and the parameters for $Pb_3(Mn_{0.95}Ge_{0.05})_7O_{15}$ and $Pb_3(Mn_{0.95}Ga_{0.05})_7O_{15}$ were found with allowance for the Curie–Weiss law.

Figure 3 shows the isothermal magnetization curves of $Pb_3Mn_7O_{15}$ recorded at various tempera-

Table 2. Atomic coordinates and isotropic/equivalent thermal parameters

Atom	x	y	z	U^*_{iso}/U_{eq}
		$Pb_3Mn_7O_{15}$		
Pb1	0.24319 (8)	0.25	0.3571 (1)	0.0128 (3)
Pb2	0.2319 (1)	0.25	0.0114 (1)	0.0158 (3)
Pb3	0.24375 (6)	0.38203 (5)	0.6124 (1)	0.0144 (3)
Pb4	0.25057 (5)	0.44395 (5)	−0.0592 (1)	0.0134 (3)
Mn1	−0.0066 (3)	0.25	−0.2463 (5)	0.0111 (9)
Mn2	0.3490 (2)	0.4171 (2)	0.2452 (3)	0.0062 (6)
Mn3	0.1433 (2)	0.4168 (2)	0.2494 (3)	0.0058 (6)
Mn4	0.4902 (3)	0.25	0.2416 (4)	0.0076 (8)
Mn5	0.5	0.5	0	0.0076 (8)
Mn6	−0.0074 (2)	0.3338 (2)	0.5013 (3)	0.0070 (6)
Mn7	0	0.5	0	0.0081 (8)
Mn8	0.50248 (19)	0.5814 (2)	0.2533 (3)	0.0074 (6)
Mn9	0.0077 (3)	0.6648 (2)	0.0083 (3)	0.0083 (6)
O1	0.066 (1)	0.25	−0.414 (2)	0.002 (3)*
O2	−0.087 (1)	0.4130 (9)	0.429 (2)	0.013 (3)*
O3	0.416 (2)	0.25	0.072 (2)	0.009 (4)*
O4	0.430 (1)	0.589 (1)	0.081 (2)	0.015 (3)*
O5	0.079 (1)	0.584 (1)	0.076 (2)	0.019 (4)*
O6	0.424 (1)	0.509 (1)	0.344 (2)	0.015 (3)*
O7	−0.079 (2)	0.25	−0.083 (2)	0.009 (4)*
O8	0.076 (1)	0.418 (1)	0.077 (2)	0.016 (3)*
O9	0.568 (1)	0.3261 (8)	0.154 (2)	0.008 (3)*
O10	0.412 (1)	0.3288 (9)	0.328 (2)	0.013 (3)*
O11	−0.081 (1)	0.3317 (9)	0.672 (2)	0.009 (3)*
O12	0.579 (1)	0.505 (1)	0.167 (2)	0.016 (3)*
O13	0.072 (1)	0.329 (1)	−0.172 (2)	0.018 (3)*
O14	0.2472 (8)	0.4246 (9)	0.401 (2)	0.004 (2)*
O15	0.233 (1)	0.336 (1)	0.184 (2)	0.016 (3)*
O16	0.257 (1)	0.493 (1)	0.164 (2)	0.010 (3)*
O17	−0.064 (2)	0.75	−0.087 (2)	0.013 (4)*
		$Pb_3Mn_7O_{15}:Ge^{4+}$		
Pb1	0.2452 (1)	0.25	0.3615 (1)	0.0146 (3)
Pb2	0.2397 (1)	0.25	0.0149 (1)	0.0180 (3)
Pb3	0.24513 (8)	0.38272 (6)	0.6170 (1)	0.0207 (3)
Pb4	0.25034 (7)	0.44419 (6)	−0.0558 (1)	0.0154 (3)

Table 2. (Contd.)

Atom	x	y	z	U^*_{iso}/U_{eq}
Mn1	−0.0047 (4)	0.25	−0.2477 (5)	0.0109 (9)
Mn2	0.3508 (2)	0.4168 (2)	0.2485 (4)	0.0076 (6)
Mn3	0.1445 (2)	0.4165 (2)	0.2513 (3)	0.0066 (6)
Mn4	0.4947 (3)	0.25	0.2455 (5)	0.0072 (8)
Mn5	0.5	0.5	0	0.0088 (8)
Mn6	−0.0048 (3)	0.3338 (2)	0.4997 (4)	0.0092 (6)
Mn7	0	0.5	0	0.0084 (8)
Mn8	0.5020 (2)	0.5813 (2)	0.2523 (3)	0.0109 (6)
Mn9	0.0052 (3)	0.6652 (2)	−0.0057 (4)	0.0103 (6)
O1	0.068 (2)	0.25	−0.412 (3)	0.018 (5)*
O2	−0.083 (1)	0.415 (1)	0.428 (2)	0.015 (3)*
O3	0.420 (2)	0.25	0.076 (3)	0.019 (5)*
O4	0.431 (1)	0.585 (1)	0.084 (2)	0.017 (3)*
O5	0.075 (2)	0.581 (1)	0.081 (2)	0.020 (4)*
O6	0.423 (1)	0.507 (1)	0.338 (2)	0.016 (3)*
O7	−0.080 (2)	0.25	−0.084 (3)	0.022 (6)*
O8	0.077 (1)	0.418 (1)	0.074 (2)	0.014 (3)*
O9	0.571 (1)	0.328 (1)	0.157 (2)	0.013 (3)*
O10	0.416 (1)	0.329 (1)	0.334 (2)	0.016 (3)*
O11	−0.079 (1)	0.332 (1)	0.670 (2)	0.015 (3)*
O12	0.580 (2)	0.504 (1)	0.166 (2)	0.018 (4)*
O13	0.072 (2)	0.331 (1)	−0.168 (2)	0.018 (4)*
O14	0.248 (1)	0.424 (1)	0.403 (2)	0.019 (4)*
O15	0.239 (1)	0.336 (1)	0.185 (2)	0.016 (3)*
O16	0.255 (1)	0.490 (1)	0.165 (2)	0.017 (4)*
O17	−0.066 (2)	0.75	−0.085 (3)	0.019 (5)*
		$Pb_3Mn_7O_{15}:Ga^{3+}$		
Pb1	0.24385 (9)	0.2500	0.35980 (12)	0.0141 (3)
Pb2	0.23600 (11)	0.2500	0.01351 (12)	0.0167 (3)
Pb3	0.24445 (7)	0.38239 (5)	0.61510 (9)	0.0170 (2)
Pb4	0.25054 (7)	0.44407 (5)	−0.05718 (9)	0.0145 (2)
Mn1	−0.0057 (3)	0.2500	−0.2468 (5)	0.0114 (9)
Mn2	0.3498 (2)	0.41688 (19)	0.2469 (3)	0.0074 (6)
Mn3	0.1443 (2)	0.41645 (18)	0.2505 (3)	0.0066 (6)
Mn4	0.4927 (3)	0.2500	0.2438 (5)	0.0077 (8)
Mn5	0.5000	0.5000	0.0000	0.0079 (8)

Table 2. (Contd.)

Atom	x	y	z	U^*_{iso}/U_{eq}
Mn6	−0.0059 (2)	0.33363 (18)	0.5004 (3)	0.0077 (6)
Mn7	0.0000	0.5000	0.0000	0.0081 (8)
Mn8	0.5025 (2)	0.58136 (19)	0.2530 (3)	0.0087 (6)
Mn9	0.0066 (3)	0.66520 (18)	−0.0070 (3)	0.0094 (6)
O1	0.0670 (18)	0.2500	−0.411 (3)	0.015 (5)*
O2	−0.0845 (12)	0.4142 (10)	0.4300 (18)	0.015 (3)*
O3	0.4180 (18)	0.2500	0.074 (3)	0.015 (5)*
O4	0.4304 (12)	0.5855 (10)	0.0823 (18)	0.016 (3)*
O5	0.0775 (13)	0.5813 (11)	0.0792 (19)	0.019 (4)*
O6	0.4216 (13)	0.5071 (10)	0.3403 (18)	0.017 (3)*
O7	−0.080 (2)	0.2500	−0.084 (3)	0.022 (5)*
O8	0.0761 (12)	0.4182 (10)	0.0751 (18)	0.015 (3)*
O9	0.5715 (12)	0.3266 (10)	0.1545 (17)	0.013 (3)*
O10	0.4138 (12)	0.3284 (10)	0.3319 (17)	0.014 (3)*
O11	−0.0772 (13)	0.3340 (10)	0.6714 (18)	0.016 (3)*
O12	0.5810 (13)	0.5033 (10)	0.1681 (19)	0.018 (4)*
O13	0.0680 (13)	0.3319 (10)	−0.1674 (19)	0.018 (3)*
O14	0.2470 (12)	0.4238 (11)	0.4012 (19)	0.018 (4)*
O15	0.2363 (12)	0.3360 (10)	0.1856 (17)	0.014 (3)*
O16	0.2570 (12)	0.4894 (11)	0.1656 (19)	0.017 (3)*
O17	−0.0659 (18)	0.7500	−0.087 (3)	0.017 (5)*

tures. Hysteresis curves for the direction $\mathbf{B} \perp \mathbf{a}$ with a coercive force of about 2 T at $T = 4.2$ K are visible. The hysteresis disappears far from the Néel temperature: it is very weak at $T > 60$ K. Up to 8 T, there is no tendency toward saturation at any temperature. The field dependence of magnetization is linear for the magnetic field direction $\mathbf{B} \parallel \mathbf{a}$.

The substitution of germanium Ge^{4+} ions for manganese Mn^{4+} ions at a low concentration only weakly changes the magnetic properties. The effective magnetic moment and the Néel temperature decrease weakly (Fig. 2b), and the paramagnetic Curie temperature decreases by a factor of 1.5 (Table 3). The strongly broadened peak at $T_1 = 160$ K in the temperature dependence is also observed (inset to Fig. 2b). The magnetization curves differ weakly from the curves of the unsubstituted composition. We can only note that the field dependences of magnetization for the direction $\mathbf{B} \parallel \mathbf{a}$ ceased to be linear and that the hysteresis for the direction $\mathbf{B} \perp \mathbf{a}$ takes place up to the magnetic ordering temperature (Fig. 4).

Table 3. Magnetic parameters of the single crystals

	T_N, K	θ, K	μ_{eff}, μ_B	μ_{theor}, μ_B
$Pb_3Mn_7O_{15}$	72	−590	13.3	11.9
$Pb_3(Mn_{0.95}Ge_{0.95})_7O_{15}$	70	−380	12	11.7
$Pb_3(Mn_{0.95}Ga_{0.95})_7O_{15}$	62	−290	11.3	11.5

The magnetic properties of $Pb_3Mn_7O_{15}$ change more substantially when gallium Ga^{3+} ions substitute for manganese Mn^{3+} ions even at a low concentration. The Néel temperature decreases by 10 K and the paramagnetic Curie temperature almost halves as compared to nominally pure $Pb_3Mn_7O_{15}$ (Table 3). The broad peak at $T_1 = 160$ K in the temperature dependence of magnetization disappears (inset to Fig. 2c). A magnetic field component appears along axis a in

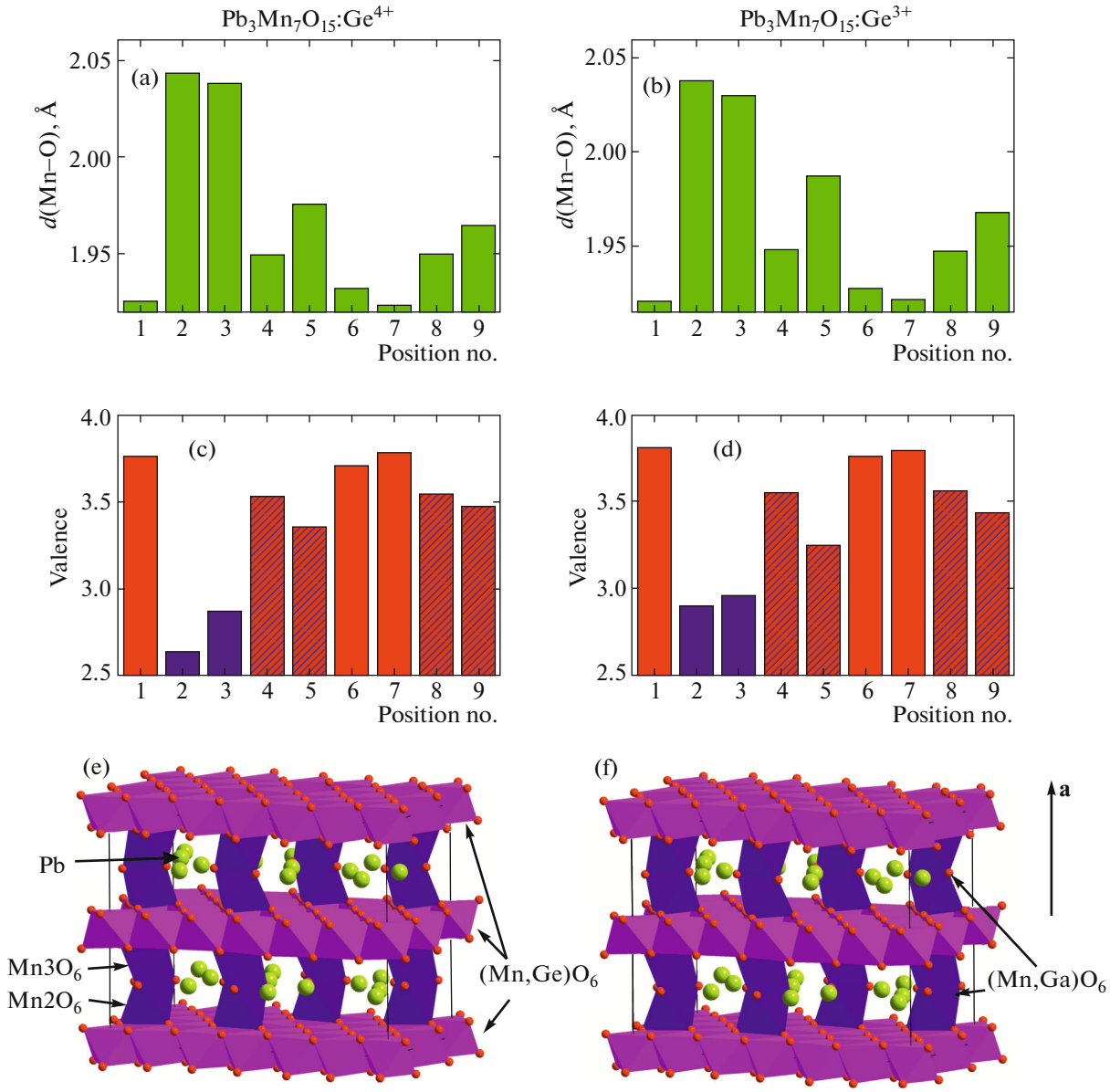

Fig. 1. (Color online) Average bond lengths d(Mn–O) for each position in (a) $Pb_3Mn_7O_{15}:Ge^{4+}$ and (b) $Pb_3Mn_7O_{15}:Ga^{3+}$. (c, d) The calculated sums of valence forces demonstrate the presence of two positions occupied by Mn^{3+} ions (short blue rectangles), three positions occupied by Mn^{4+} (high red rectangles), and other mixed Mn^{3+}/Mn^{4+} positions (hatched rectangles). Correspondingly, the Ge^{4+} ions in $Pb_3Mn_7O_{15}:Ge^{4+}$ predominantly occupy the positions in layers (e) and the Ga^{3+} ions occupy the positions in the columns between the layers (f).

weak magnetic fields, and we cannot now state unambiguously that the magnetic moment lies in the *bc* plane (Fig. 2c). The hysteresis in the field dependences of magnetization of $Pb_3Mn_7O_{15}$ and $Pb_3(Mn_{0.95}Ge_{0.05})_7O_{15}$ is absent for $Pb_3(Mn_{0.95}Ga_{0.05})_7O_{15}$ (Fig. 5). The field dependences measured in the directions $\mathbf{B} \perp \mathbf{a}$ and $\mathbf{B} \parallel \mathbf{a}$ became close in shape and value; that is, the addition of 5 wt % Ga^{3+} leads to a significant transformation of the magnetic properties of $Pb_3Mn_7O_{15}$.

To interpret these results, it is necessary to take into account that the crystal structure of $Pb_3Mn_7O_{15}$ has a well-pronounced layered character. The manganese ions located in an octahedral oxygen environment form layers in the *bc* plane, which are connected by bridges consisting of two oxygen octahedra (Fig. 1). If a nonmagnetic ion is incorporated in such a column (bridge) instead of a manganese ion, the exchange coupling between the layers should be broken. In turn,

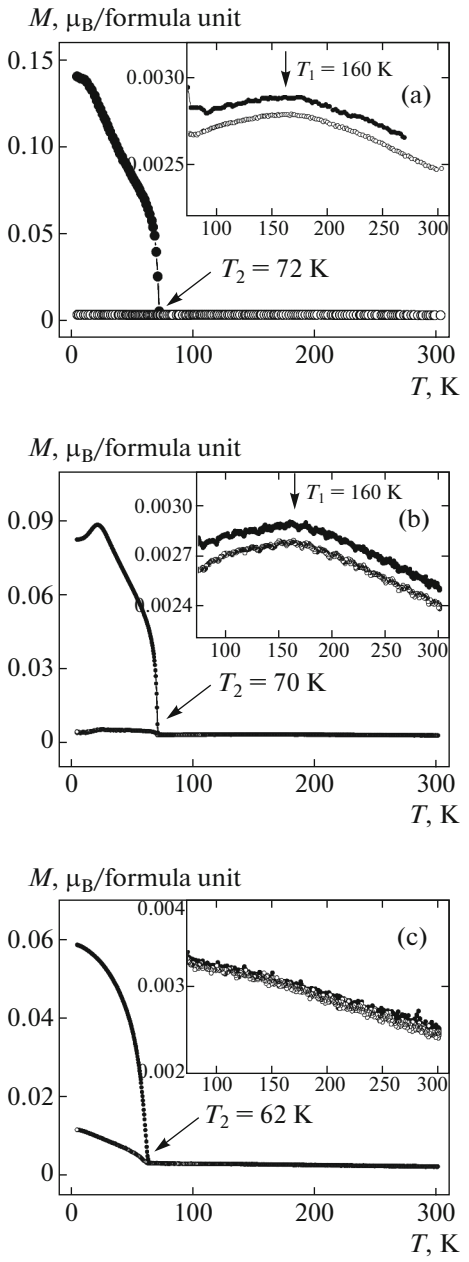

Fig. 2. Temperature dependences of magnetization recorded upon cooling in a magnetic field $B = 0.05$ T for (a) $Pb_3Mn_7O_{15}$, (b) $Pb_3(Mn_{0.95}Ge_{0.05})_7O_{15}$, and (c) $Pb_3(Mn_{0.95}Ga_{0.05})_7O_{15}$. (solid circles) Magnetic field lying in the *bc* plane and (open circles) magnetic field lying along the a axis. (inset) Enlarged curves.

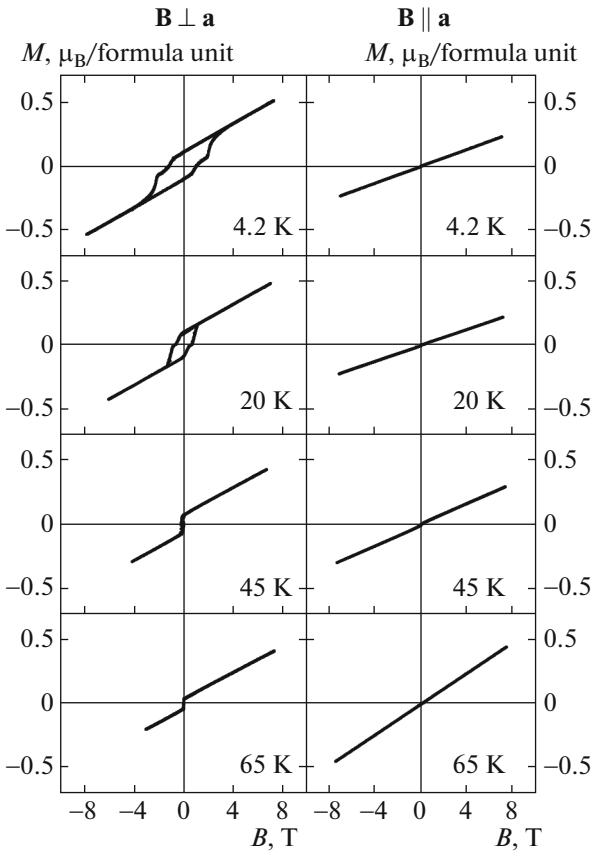

Fig. 3. Field dependences of magnetization for $Pb_3Mn_7O_{15}$ and the orientations $\mathbf{B} \perp \mathbf{a}$ and $\mathbf{B} \parallel \mathbf{a}$ at various temperatures.

this break should result in a decrease in the magnetic order parameter (which is equivalent to a decrease in T_N) and the exchange interaction (which is determined by paramagnetic Curie temperature θ) and should change the magnetic anisotropy upon changing the local symmetry of an electric field. Of course, these changes could manifest themselves when a nonmagnetic ion is placed in the *bc* plane; however, a break in the exchange coupling in the columns would result in a higher effect. Based on the results presented above, we can draw an unambiguous conclusion that the columns only have manganese ions in the trivalent state (Mn^{3+}) substituted by gallium Ga^{3+} ions. Ge^{4+} ions substitute for the Mn^{4+} ions located in the *bc* layers.

4. DISCUSSION OF RESULTS

Before analyzing the exchange magnetic structure of $Pb_3Mn_7O_{15}$, we use the following assumptions. As noted above, a $Pb_3Mn_7O_{15}$ crystal has orthorhombic symmetry *Pnma* at room temperature or below, manganese ions are situated in nine nonequivalent positions, and the unit cell has 56 manganese ions (eight formula units) [5]. This structure differs from the hexagonal $P6_3/mcm$ structure only in small displacements of cations and anions [6]. The integral of cation–cation exchange interaction (its sign and value) is mainly determined by the occupancy of individual orbitals. Here, the interionic distances and the bond angles play only a minor role: they only weakly change the integral and do not change the initial mag-

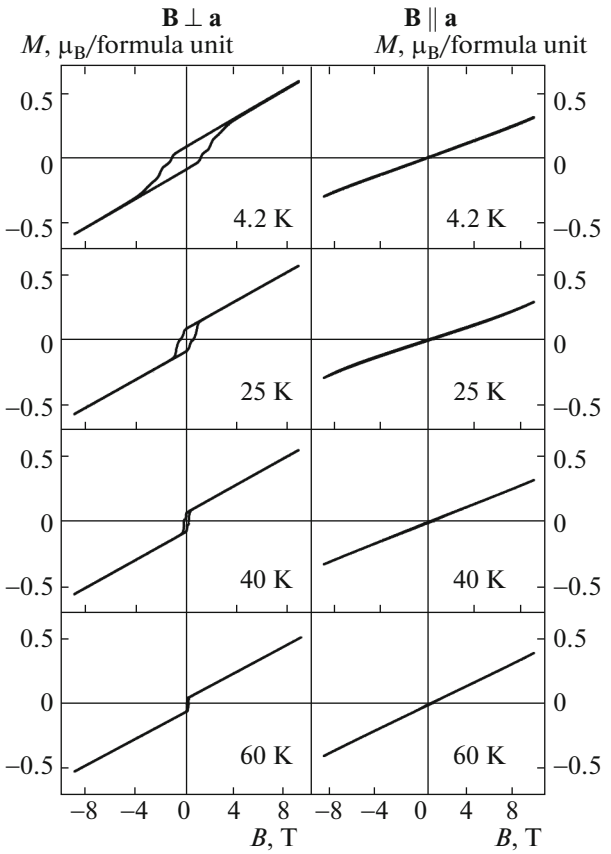

Fig. 4. Field dependences of magnetization for $Pb_3(Mn_{0.95}Ge_{0.05})_7O_{15}$ and the orientations **B** ⊥ **a** and **B** ∥ **a** at various temperatures.

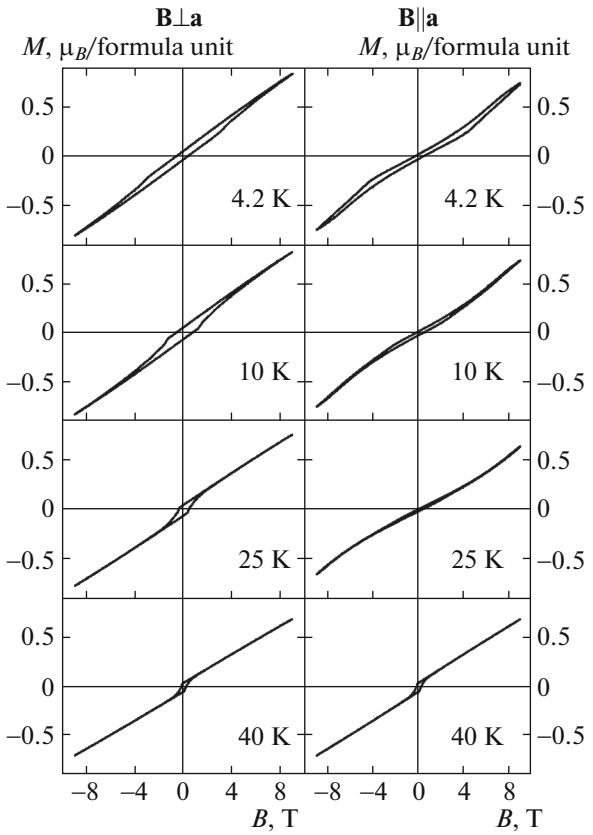

Fig. 5. Field dependences of magnetization for $Pb_3(Mn_{0.95}Ga_{0.05})_7O_{15}$ and the orientations **B** ⊥ **a** and **B** ∥ **a** at various temperatures.

netic structure. Therefore, we analyzed the magnetic state of $Pb_3Mn_7O_{15}$ using the hexagonal $P6_3/mcm$ structure (four formula unit), which is simpler for analysis and is inherent in this compound at a temperature above 560 K. In this case, the nonequivalent positions in the orthorhombic *Pnma* structure transform into the nonequivalent positions in the hexagonal structure, as is shown in Fig. 4.

Figure 6 shows the image of the hexagonal $P6_3/mcm$ structure where only manganese ions are depicted. Note that axis *c* is now preferred (instead of axis *a* in space group *Pnma*) and plane *ab* is an easy magnetization plane.

For a correct calculation, first of all we have to determine the valences of the Mn ions in each nonequivalent position. The problem seems to be nontrivial, since, from a theoretical standpoint, Mn ions in the Mn^{3+} and Mn^{4+} states or in a mixed valence state can be located in any nonequivalent position. The hexagonal packing of $Pb_3Mn_7O_{15}$ has four nonequivalent positions of manganese ions: positions Mn1(12*i*), Mn3(6*f*), and Mn4(2*b*) are located in the *ab* planes connected by the columns consisting of two oxygen octahedra forming position Mn2(8*h*) (Fig. 6) [2]. Using the data from [8] (where trivalent iron Fe^{3+} ions were shown to occupy positions Mn1(12*i*), Mn2(8*h*), and Mn3(6*f*)), we assumed that Mn^{3+} ions occupy these positions as well. The presence of Jahn–Teller Mn^{3+} ions in these positions should distort the oxygen octahedra containing these ions, which basically follows from the crystallographic data [6]. In contrast, Mn^{4+} ions should an almost ideal oxygen octahedron around them. Such octahedra are characteristic of position Mn4(2*b*). The distribution of Mn ions of different valences over different nonequivalent positions was described by Kimber [7], who used the empirical method of summing valence forces. Based on the data described above and the results from [7, 8], we chose the following model: positions Mn1(12*i*) and Mn3(6*f*) contain both Mn^{3+} and Mn^{4+} ions; position Mn4(2*b*), which has an ideal oxygen octahedron, contains Mn^{4+} ions; and the most strongly distorted oxygen octahedron of position Mn2(8*h*) has Mn^{3+} ions. This assumption agrees fully with the results of our magnetic investigations performed on substituted $Pb_3Mn_7O_{15}$ compositions. As a result, the final formula for $Pb_3Mn_7O_{15}$ in the hexagonal representation per formula unit can be written as

$$Pb_3[Mn1_x^{3}Mn1_{3-x}^{4+}Mn2_2^{3+}Mn3_y^{3+}Mn3_{1.5-y}^{4+}Mn4_{0.5}^{4+}]O_{15}, \quad (1)$$

where x and y are connected by the relation $x = 2 - y$ (with allowance for the electroneutrality of the formula). As follows from [8], the number of Mn^{3+} ions should be at least higher than one-fourth of the total number of Mn ions in position Mn3(6*f*) (since at least one-fourth in this position is occupied by Fe^{3+} ions in the $Pb_3(Mn_{0.85}Fe_{0.15})O_{15}$ compound) or $y > 0.375$. Thus, y can change in the range {0.375, 1.5}; whence, it follows that the ratio Mn^{4+}/Mn^{3+} in position Mn3(6*f*) can change in the range {3, 0}. x can change in the range {1.625, 0.5}; that is, the ratio Mn^{4+}/Mn^{3+} in position Mn1(12*i*) can change in the range {11/13, 5}.

The exchange interactions were estimated in terms of the indirect coupling model [14–16]. This model can be used to estimate the entire set of cation–cation interactions in a crystal. In turn, the knowledge of the exchange interactions makes it possible to predict a magnetic structure and magnetic ordering temperature. We take into account only the interactions with the nearest neighbors, i.e., the short Mn–O–Mn bonds, and neglect the long Mn–O–B(Pb)–O–Mn bonds. In this approximation, the magnetic system of $Pb_3Mn_7O_{15}$ is described by the following set of indirect exchange parameters.

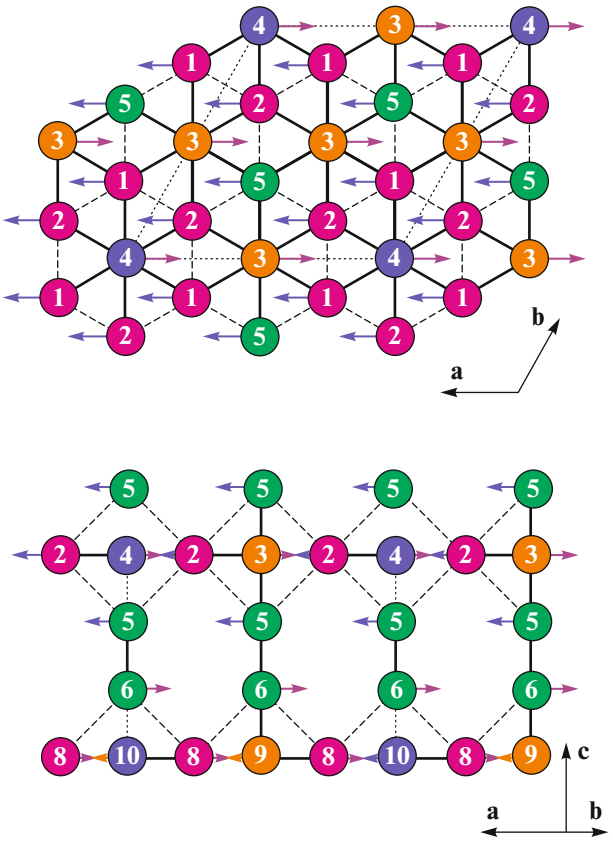

Fig. 6. (Color online) Schematic image of the magnetic structure of $Pb_3Mn_7O_{15}$. (red circles) Magnetic sublattices 1, 2, 3, and 4 correspond to position 12*i*; (yellow circles) sublattices 3 and 9, to 8*f*; (blue circles) 4 and 10, to 2*b*; and (green circles) 5 and 6, to 8*h*. The solid lines correspond to the exchange interaction that determines the magnetic structure, and the dashed lines correspond to a frustrated exchange interaction. The dotted lines illustrate the unit cell.

The parameters characterizing the intralayer exchange interactions are as follows:

$$J_{4d-4d}^{12i12i}(90) = -\frac{1}{8}c\left[2(b+c)U_4 - \frac{5}{3}bJ_4\right] = -5.9\ \text{K},$$

$$J_{4d-3d}^{12i12i}(90) = -\frac{1}{12}c\left[(b+2c)(U_3+U_4) - \frac{1}{3}b(8J_3+5J_4)\right] = -4.7\ \text{K},$$

$$J_{3d-3d}^{12i12i}(90) = -\frac{4}{9}c\left[2U_3 - \frac{4}{3}bJ_3\right] = -1.6\ \text{K},$$

$$J_{4d-4d}^{12i6f}(90) = -\frac{1}{4}c\left[\left(\frac{4}{3}b + c\right)U_4 - \frac{2}{3}bJ_4\right] = -7.9\ \text{K},$$

$$J_{4d-3d}^{12i6f}(90) = -\frac{1}{12}c\left[2\left(\frac{4}{3}b + c\right)(U_3 + U_4) - b\left(J_3 + \frac{5}{3}J_4\right)\right] = -11\ \text{K},$$

$$J_{3d-4d}^{12i6f}(90) = -\frac{1}{12}c\left[\left(\frac{5}{3}b + 2c\right)(U_3 + U_4) - b\left(\frac{8}{3}J_3 + J_4\right)\right] = -7.3\,\text{K},$$

$$J_{3d-3d}^{12i6f}(90) = -\frac{1}{9}c\left[2\left(\frac{5}{3}b + 2c\right)U_3 - \frac{11}{3}bJ_3\right] = -10.3\ \text{K},$$

$$J_{4d-3d}^{12i2d}(90) = -\frac{1}{6}c\left[(b+c)(U_3+U_4) - \frac{1}{3}b(4J_3+J_4)\right] = -8.6\ \text{K},$$

$$J_{3d-3d}^{12i2d}(90) = -\frac{4}{9}c\left[cU_3 - \frac{4}{3}bJ_3\right] = -1.6\ \text{K}.$$

The parameters characterizing the interlayer exchange interactions are as follows:

$$J_{4d-4d}^{12i8h}(128) = -\frac{1}{16}\left(4c^2U_4 - \frac{4}{3}b^2J_2\right)|\cos 128^\circ| = -0.8\ \text{K},$$

$$J_{3d-4d}^{12i8h}(128) = -\frac{1}{6}\left(c^2(U_3+U_4) - \frac{2}{3}b^2J_3\right)|\cos 128^\circ| = -1.4\ \text{K},$$

$$J_{4d-4d}^{8h8h}(135) = -\frac{1}{16}c((8c+14b)U_4 - bJ_4)|\cos 135^\circ| = -15.4\ \text{K},$$

Table 4. Correspondence between the nonequivalent positions in the orthorhombic *Pnma* and hexagonal $P6_3/mcm$ structures. The Mn ion coordinates in the $P6_3/mcm$ structure were taken from the ICSD database (file 183992)

Pnma		$P6_3/mcm$				
Atom	Position	Atom	Position	*x*	*y*	*z*
Mn6	8*d*	Mn1	12*i*	0.8314(1)	0.1686(1)	1/2
Mn8	8*d*					
Mn9	8*d*					
Mn2	8*d*	Mn2	8*h*	1/3	2/3	0.1468(2)
Mn3	8*d*					
Mn4	4*a*	Mn3	6*f*	1/2	1/2	1/2
Mn5	4*b*					
Mn7	4*a*					
Mn1	4*c*	Mn4	2*b*	0	0	0

Table 5. Parameters of the intersublattice interaction in $Pb_3Mn_7O_{15}$

	$Z_{ij}J_{ij}$, K			
	$M_1(12i)\ \langle S_1\rangle = 5/3$	$M_2(6f)\ \langle S_2\rangle = 11/6$	$M_3(2d)\ \langle S_3\rangle = 3/2$	$M_4(8h)\ \langle S_4\rangle = 2$
$M_1(12i)\ \langle S_1\rangle = 5/3$	−6.91	−17.02	−3.93	−1
$M_2(6f)\ \langle S_2\rangle = 11/6$	−34.04	0	0	−3
$M_3(2d)\ \langle S_3\rangle = 3/2$	−23.6	0	0	0
$M_4(8h)\ \langle S_4\rangle = 2$	−3.6	−5.1	0	−15

Table 6. Exchange interactions in $Pb_3Mn_7O_{15}$. Ordering interactions are placed in bold type and frustrated interactions, in italic type

J_{ij}, K	no. 1 ↑	no. 2 ↑	no. 3 ↓	no. 4 ↓	no. 5 ↑	no. 6 ↓	no. 7 ↓	no. 8 ↓	no. 9 ↑	no. 10 ↑
no. 1, ↑	0	*−6.9*	**−17**	**−3.9**	*−1.2*	0	0	0	0	0
no. 2, ↑	*−6.9*	0	**−17**	**−3.9**	*−1.2*	0	0	0	0	0
no. 3, ↓	**−34**	**−34**	0	0	**−3.4**	0	0	0	0	0
no. 4, ↓	**−23.6**	**−23.6**	0	0	0	0	0	0	0	0
no. 5, ↑	*−3.6*	*−3.6*	**−5.1**	0	0	**−15.4**	0	0	0	0
no. 6, ↓	0	0	0	0	**−15.4**	0	*−3.6*	*−3.6*	**−5.1**	0
no. 7, ↓	0	0	0	0	0	*−1.2*	0	*−6.9*	**−17**	**−3.9**
no. 8, ↓	0	0	0	0	0	*−1.2*	*−6.9*	0	**−17**	**−3.9**
no. 9, ↑	0	0	0	0	0	−3.4	**−34**	**−34**	0	0
no. 10, ↑	0	0	0	0	0	0	**−23.6**	**−23.6**	0	0

$$J_{4d-4d}^{8h6f}(125) = -\frac{1}{4}\left(\left(c^2+\frac{2}{9}b^2\right)U_4 - \frac{1}{3}b^2J_4\right)|\cos 125^\circ| = -2 \text{ K},$$

$$J_{4d-3d}^{8h6f}(125) = -\frac{1}{6}\left(c^2(U_3+U_4) - \frac{8}{9}b^2J_3\right)|\cos 125^\circ| = -1.1 \text{ K}.$$

In these formulas, the subscripts of the exchange interaction integral mean the state of the electron shell of interacting cations (4*d* for Mn^{3+}, 3*d* for Mn^{4+}), and the superscripts mean the positions occupied by them. The indirect bond angles are given in the parentheses near the integrals; *b* and *c* are the parameters of electron transport along σ and π bonds, respectively; U_3 and U_4 are the energies of the ligand–cation electron excitation; and J_3 and J_4 are the intraatomic exchange integrals, respectively. As basic parameters, we took the parameters that are characteristic of spinel-type multisublattice oxide compounds [13],

$$b \sim 0.02, \quad U_3 \sim 9 \text{ eV}, \quad J_3 \sim 2.2 \text{ eV},$$
$$c \sim 0.01, \quad U_4 \sim 8.5 \text{ eV}, \quad J_4 \sim 3 \text{ eV}.$$

In principle, knowing the intersublattice interactions, we can calculate the Néel temperature. To estimate the intersublattice interactions, we have to know the distribution of cations of different valences over crystallographic positions, i.e., *x* or *y* in Eq. (1). When varying parameter *y*, we found that the calculated Néel temperature was in agreement with the experimentally determined temperature (T_N = 72 K) at *y* = 1 (this value falls in the determined range of possible values of *y* {0.375, 1.5}). For simplification, we reduced the number of magnetic sublattices to the number of crystallographic sublattices. As a result, Eq. (1) for $Pb_3Mn_7O_{15}$ can be written in the following form in the hexagonal representation for the calculation per formula unit:

$$Pb_3[Mn1_1^{3+}Mn1_2^{4+}Mn2_2^{3+}Mn3_1^{3+}Mn3_{0.5}^{4+}Mn4_{0.5}^{4+}]O_{15}. \quad (2)$$

It is seen that the Mn^{4+}/Mn^{3+} ratio is 2 : 1 for position Mn1(12*i*) and 1 : 2 for position Mn3(6*f*). Table 5 presents the parameters of the intersublattice exchange interactions for $Pb_3Mn_7O_{15}$ with the manganese ion distribution Mn^{4+}/Mn^{3+} taken from Eq. (2).

Knowing the manganese ion distribution Mn^{3+}/Mn^{4+} in each nonequivalent position, we now analyze the mole concentration structure of $Pb_3Mn_7O_{15}$. To this end, we divide the magnetic ions into sublattices (see Fig. 6). Sublattices 1, 2, 7, and 8 occupy position 12*i*; sublattices 3 and 9, position 6*f*; 4 and 10, 2*b*; and 6, 8*h*. Magnetic sublattices 1–4 are located in one *ab* plane, sublattices 7–10 are located in neighboring *ab* planes, and they differ only in the opposite direction of the magnetic moment. We now calculate the energies of the intersublattice exchange interactions by taking into account the numbers of bonds and the position occupancy by Mn^{3+} and Mn^{4+} cations (Table 6). The ratios of these interactions can be used to determine the mutual orientation of the magnetic moments of various positions. These orientations are indicated by arrows in the table.

All exchange interactions between cations are seen to be antiferromagnetic. Note that strong geometric frustrations explain the relatively low ordering temperature (T_N = 72 K) in the presence of a strong exchange interaction (θ = –590 K). The frustration interactions are represented by the interactions between magnetic sublattices 1 and 2 (7 and 8) and 1, 2, and 5 (7, 8, and 6). The other interactions determine the magnetic structure of the compound.

The total magnetic moment per formula unit in the *ab* plane with allowance for only the spin moment of Mn ions ($S_{Mn^{3+}} = 2\mu_B$, $S_{Mn^{4+}} = 3/2\mu_B$) is calculated as follows:

$$M_{\text{plane}} = (1S_{Mn1^{3+}} + 2S_{Mn^{4+}}) - \left(1S_{Mn3^{3+}} + \frac{1}{2}S_{Mn^{4+}} + \frac{1}{2}S_{Mn4^{4+}}\right) = 3\mu_B. \quad (3)$$

Thus, the magnetic structure of $Pb_3Mn_7O_{15}$ can be interpreted as follows. The magnetic layers that contain manganese ions in positions 12*i*, 6*f*, and 2*b* are connected to the same layers through columns, which contain two manganese ions in position 8*h* and do not interact with each other (sublattices 5, 6). Since the exchange interaction between two neighboring manganese ions in these positions is negative (J_{4d-4d}^{8h8h}), it is obvious that the total magnetic moments of the neighboring planes are antiparallel. Finally, we can state that $Pb_3Mn_7O_{15}$ is antiferromagnetic with a frustrated magnetic structure.

CONCLUSIONS

$Pb_3(Mn_{0.95}Ge_{0.05})_7O_{15}$ and $Pb_3(Mn_{0.95}Ga_{0.05})_7O_{15}$ single crystals were grown using spontaneous solidification from a molten solution. The lattice parameters and the crystal structure of these single crystals were determined by XRD. Both compounds have an orthorhombic structure with space group *Pnma*. The magnetic properties of these single crystals were studied and compared with those of nominally pure $Pb_3Mn_7O_{15}$.

It was found that the substitution of germanium Ge^{4+} ions for manganese Mn^{4+} ions at a low concentration (5 at %) did not cause a substantial change in the magnetic properties. The effective magnetic moment and the Néel temperature slightly decreased, and the strongly broadened in the temperature dependence of magnetization at *T* = 160 K was retained. The magnetization curves differed slightly from the curves of the unsubstituted composition.

The substitution of Ga^{3+} ions for manganese Mn^{3+} ions at a concentration of 5 at % substantially changed the magnetic properties. The Néel temperature decreased by 10 K and the paramagnetic Curie temperature almost halved. The broad peak at $T_1 = 160$ K in th eutectoid of magnetization disappeared and the magnetic anisotropy changed substantially.

The indirect-coupling model was used to analyze the exchange interactions in $Pb_3Mn_7O_{15}$ in the hexagonal setting. Using this model, we were able to qualitatively explain the change in the magnetic properties of a $Pb_3Mn_7O_{15}$ single crystal doped with gallium or germanium ions. The radical change in the magnetic structure in $Pb_3(Mn_{0.95}Ga_{0.05})_7O_{15}$ was found to be mainly caused by the presence of gallium ions in position 8*h*, which leads to a break in the coupling of the interplanar exchange interaction through the columns connecting ferromagnetically ordered planes. The ratios of manganese ions Mn^{4+}/Mn^{3+} in each nonequivalent position in $Pb_3Mn_7O_{15}$ were determined.

ACKNOWLEDGMENTS

This work was performed in terms of a state task of the Ministry of Education and Science of the Russian Federation to Siberian Federal University (project no. 3.2534.2014/K).

REFERENCES

1. K. H. Kim, M. Uehara, V. Kiryukhin, and S. W. Cheong, *Colossal Magnetoresistive Manganites,* Ed. by T. Chatterji (Kluwer-Academic, Dordrecht, 2004).
2. N. V. Volkov, K. A. Sablina, O. A. Bayukov, et al., J. Phys.: Condens. Matter **20**, 055217 (2008).
3. N. V. Volkov, K. A. Sablina, E. V. Eremin, et al., J. Phys.: Condens. Matter **20**, 445214 (2008).
4. N. V. Volkov, E. V. Eremin, K. A. Sablina, et al., J. Phys.: Condens. Matter **22**, 375901 (2010).
5. J. C. E. Rash, D. V. Sheptyakov, J. Schefer, et al., J. Solid State Chem. **182**, 1188 (2009).
6. N. V. Volkov, L. A. Solovyov, E. V. Eremin, et al., Physica B **407**, 689 (2012).
7. S. A. J. Kimber, J. Phys.: Condens. Matter **24**, 186002 (2012).
8. N. V. Volkov, E. V. Eremin, O. A. Bayukov, et al., J. Magn. Magn. Mater. **342**, 100 (2013).
9. A. J. Gatimu, H. Mizoguchi, A. Sleight, et al., J. Solid State Chem. **183**, 866 (2010).
10. T. I. Milenov, P. M. Rafailov, V. Tomov, et al., J. Phys.: Condens. Matter **23**, 156001 (2011).
11. G. M. Sheldrick, Acta Crystallogr. A **64**, 112 (2008).
12. R. D. Shannon, Acta Crystallogr. A **32**, 751 (1976).
13. I. D. Brown and D. Altermatt, Acta Crystallogr. B **41**, 244 (1985).
14. P. W. Anderson, Phys. Rev. **115**, 1 (1959).
15. M. V. Eremin, Sov. Phys. Solid State **24**, 239 (1982).
16. A. Bayukov and A. F. Savitskii, Phys. Solid State **36**, 1049 (1994).

Translated by K. Shakhlevich